Title

D-loop Dynamics and Near-Atomic-Resolution Cryo-EM Structure of Phalloidin-Bound F-Actin

Permalink

Journal

ISSN

Authors

Das, Sanchaita
Ge, Peng
Oztug Durer, Zeynep A
et al.

Publication Date

DOI

Peer reviewed

D-loop dynamics and near-atomic resolution cryoEM structure of phalloidin bound F-actin

Sanchaita Das[1], **Peng Ge**[2], **Zeynep A. Oztug Durer**[1,#], **Elena E. Grintsevich**[1,##], **Z. Hong Zhou**[2,3,4], **Emil Reisler**[1,4,5,*]

[1]Department of Chemistry and Biochemistry, University of California, Los Angeles (UCLA), California 90095, USA

[2]California NanoSystems Institute (CNSI), UCLA, Los Angeles, California 90095, USA

[3]Department of Microbiology, Immunology and Molecular Genetics, UCLA, Los Angeles, California 90095, USA

[4]Molecular Biology Institute, UCLA, Los Angeles, California 90095, USA

[5]Lead Contact.

Summary

Detailed molecular information on G-actin assembly into filaments (F-actin), and their structure, dynamics and interactions, is essential for understanding their cellular functions. Previous studies indicate that a flexible DNase I binding loop (D-loop, residues 40–50) plays a major role in actin's conformational dynamics. Phalloidin, a "gold standard" for 6 actin filaments staining, stabilizes them and affects the D-loop. Using disulfide cross-linking in yeast actin D-loop mutant Q41C/V45C, light scattering measurements, and cryoEM reconstructions we probed the constraints of D-loop dynamics and its contribution to F-actin formation/stability. Our data support a model of residues 41–45 distances which facilitate G- to F-actin transition. We report also a 3.3 Å resolution structure of phalloidin-bound F-actin in the ADP-Pi-like (ADP-BeFx) state. It shows the phalloidin binding site on F-actin and how the relative movement between its two protofilaments is restricted by it. Together, our results provide molecular details of F-actin structure and D-loop dynamics.

e-TOC Blurb:

Actin plays crucial roles in biological systems and its DNase 1 binding loop interacts with several actin binding proteins. Das *et al.* demonstrate that phalloidin (phalllotoxin) "glues" the two strands of actin filaments through additional contacts between protomers

Introduction

Actin dynamics, polymerization, depolymerization, and the remodeling of its assembled forms play a key role in many cellular processes (Neuhaus et al., 1983). Thus, a detailed molecular and structural description of the mechanisms that regulate actin structures is essential for understanding its cellular interactions and functions. The structural flexibility and mobility of some of its domains is evident in numerous atomic resolution structures of G-actin (Kabsch et al., 1990, Dominguez and Holmes, 2011, Pollard, 2016, 2017). Normal mode analysis attributes such movements to loop elements in subdomains of actin, such as its DNase I binding loop (D-loop; residues 40–50), hydrophobic loop (H-loop; residues 264–273), C-terminus (including residues 374 and 375), and the W-loop (residues 165–172) (Tirion and ben-Avraham, 1993). Cysteine mutagenesis in combination with chemical cross-linking approaches has been utilized to document the innate flexibility of these subdomains in G- and F-actin (Kim and Reisler, 1996,1998).

Several crystal structures of G-actin reveal disordered D-loop and C terminus (Kim et al., 1998, Graceffa and Dominguez, 2003, McLaughlin et al.,1993, Robinson et al.,1999) suggesting their intrinsic flexibility. Other studies show that the D-loop can adopt different secondary conformations; a β-strand in the actin complex with DNase I (Kabsch et al., 1990), a short α-helix (Otterbein et al., 2001) in the crystal structure of ADP-actin, and a disordered form in the ATP bound state (Graceffa and Dominguez, 2003). Molecular dynamics (MD) simulations of ATP- and ADP-G-actin suggest that the D-loop can transition to a helical structure (Zheng et al., 2007), but cysteine scanning mutagenesis paired with spin labeling (Durer et al., 2012) reveals that if it exists, this state is not predominant and may exist only transiently. Other studies also show a highly unstable nature of this helix in different nucleotide bound states (Zheng et al., 2007, Dalhaimer et al., 2008, Saunders et al., 2014), and/or do not detect it at all (Rould et al., 2006).

Monomeric G-actin contains bound nucleotide (ATP) and divalent cation as cofactors. Actin polymerization is accompanied by ATP hydrolysis followed by the release of gamma-phosphate (Pi) (Pollard, 2016). Some actin binding proteins are reported to have different affinity towards different nucleotide bound states of actin (Paavilainen et al., 2004). Previous studies suggest that ATP and ADP-Pi bound filaments are less flexible and more stable than ADP-bound F-actin (Orlova and Egelman, 1992, 1993), and that their severing by cofilin is attenuated (Suarez et al., 2011). A model of F-actin based on X-ray diffraction data suggests that the G- to F-actin transition involves: (i) domain movements in G-actin which facilitate F-actin formation, and (ii) an open and extended D-loop conformation in F-actin (as compared to that in G-actin (Oda et al., 2009)). Recent advances in high-resolution cryoEM investigations and biochemical studies provide snapshots of F-actin in its different states (Merino et al., 2018, Chou and Pollard, 2019, Galkin et al., 2015). They reveal differences in the conformation and location of the D-loop (Figure 1) and confirm its plasticity that was

shown in previous publications (Oztug Durer et al., 2010, Durer et al., 2012, Kotila et al., 2018). High-resolution structures of F-actin with the various bound nucleotides also suggest that the D-loop helps in stabilizing inter-protomer contacts within the filament (Merino et al., 2018, Chou and Pollard, 2019). Conversely, D-loop perturbation, as in Mical oxidized actin, can lead to F-actin disassembly (Grintsevich et al., 2017). Notably, the toxin phalloidin compensates for D-loop related polymerization defects by introducing additional inter-protomer contacts (Oda et al., 2005).

Clearly, the plasticity and conformational state of the D-loop impacts the G- to F-actin transition. To test the filaments constraints on D-loop span/confirmation, we use a double cysteine D-loop mutant Q41C/V45C of yeast actin. We probe the effect of variable length cross-linkings between these two residues on G- to F-actin transition and filaments stability. A similar approach was used before to test the H-loop (a.a. 262–274) states in yeast F-actin and revealed that trapping the loop in a transient "parked" position (by cross-linking C180 to C269 with short span reagents) disrupted the filaments (Shvetsov et al., 2006). In this study we also use negative stain electron microscopy (NS-EM) and cryo-electron microscopy (cryoEM) to obtain a structure, at 3.3 Å resolution, of F-actin-phalloidin in the ADP-Pi like state (mimicked by ADP.BeFx) i.e., in the most stable form of actin filaments.

Results

This study aims to probe D-loop plasticity and its importance in filaments formation and stability. We utilized a double cysteine mutant C41/C45 which can be constrained by cross-linking to different width. This allows us to assess the minimal C41-C45 distance that facilitates G- to F-actin transition. Additionally, we observed that phalloidin, a common reagent used to stabilize F-actin, was able to overcome a polymerization defect that was caused by C41-C45 cross-linking in the D-loop mutant. This led us to obtain a near-atomic resolution structure of actin bound to phalloidin and BeFx. Although the interaction of actin with phalloidin was mapped in a previous actomyosin structure publication (Mentes et al., 2018), we show here the actin-phalloidin complex structure without other proteins bound to it.

Cross-linking of C41 to C45 in yeast actin mutant and its effect on actin assembly

Previous studies (Oztug Durer et al., 2010) indicated that single residue yeast actin mutants Q41C and V45C had polymerization rates comparable to that of wild type actin. These mutants' residues were also found to be involved in inter-protomer contacts by cross-linking them with C265 and C374 of neighboring subunits. Here, we utilize disulfide cross-linking between C41 and C45 of the D-loop double mutant to see whether it affects G- to F-actin polymerization. The disulfide formation was catalyzed by addition of $CuSO_4$ to G- or F-actin. As monitored by light scattering and electron microscopy imaging the cross-linked G-actin was unable to polymerize into filaments after addition of $MgCl_2$ (Supplementary Figure 1). Addition of $CuSO_4$, to mutant F-actin destroyed the filaments (Figure 2A and 2Bii), but they could be rescued by addition of phalloidin (Figure 2A, 2Biv, and Supplementary Figure 1) or 10mM DTT (not shown). In contrast to phalloidin, BeFx did not promote the polymerization of disulfide cross-linked actin (Figure 2A and 2Biii).

Comparison of helical D-loop in G-actin (Figure 1A) and in several F-actin (Figure 1B) structures showed flexibility in the D-loop region. Specifically, we measured the Cα-Cα distance between C41 and C45 for each structure and noticed a change in that distance between the G- and F-actin states (Figure 1C, Supplementary Table 1). The 2D interaction map using LigPlot[+] (Laskowski and Swindells, 2011) of D-loop residues C41/C45 suggests how these residues interact with other domains of G- and F-actin in different nucleotide bound states (Supplementary Figure 2A, B, C) and in the presence of a bound phalloidin. Our structure-based analysis of the D-loop helped us to choose MTS reagents that were able to cross-link residues C41 to C45 at distances ranging from 5.4Å (MTS1) to 13Å (MTS8) (Figure 1D).

Our double cysteine mutant of actin pre-incubated with MTS1 (span of ~ 5.4 Å) was unable to polymerize after addition of $MgCl_2$, (Figure 3A and 3Cii). To investigate whether this defect was due to elongation or nucleation inhibition, the MTS1 experiment was supplemented with seeds of uncross-linked actin filaments. MTS1 cross-linked actin monomers failed to elongate from these seeds in the presence of Mg^{2+} (Figure 3B). We then tested other MTS cross-linkers, with increasing average arm length: MTS3 (span of ~6 Å), MTS6 (span of ~10 Å, Figure 3A) and MTS8 (span of ~13 Å, Figure 3A and 3Ci) and monitored their ability to form polymers by light scattering and EM. Like MTS1 treated actin, MTS3 cross-linked monomers were unable to form filaments (not shown), but MTS6 (Figure 3A) and MTS8 (Figure 3A, 3Ci) cross-linked actin monomers readily polymerized into filaments. To test whether the change in cross-linking distance also affects filament stability, we first polymerized actin with 2mM $MgCl_2$ under non-reducing conditions (Figure 3B), and then supplemented the reaction with equimolar MTS1 (Figure 3B) or MTS3 (data not shown). Addition of either $CuSO_4$ (Figure 2A), MTS1 or MTS3 led to destruction of preformed filaments. When $CuSO_4$ or MTS1 treated sample were analyzed by negative stain, we saw no traces of actin filaments (Figures 2Bii and 3Ciii).

CryoEM of the actin-phalloidin complex

We used high-resolution cryoEM to obtain a three-dimensional structure of purified ADP-BeFx-F-actin in complex with phalloidin. The filaments appear straight and/or slightly curved in the collected images (Figure 4A). Despite the presence of unbound ligands and BeFx in the background, F-actin can be seen in the aligned and averaged stacks (Figure 4A). By using Iterative Helical Real-Space Refinement (IHRSR) method (Egelman, 2010) implemented within the Relion 3 (He and Scheres, 2017) framework (Ge et al., 2014), we reconstructed a three-dimensional structure of F-actin at a resolution of 3.3 Å (Figure 4B-C, Supplementary Figure 3). The map was reconstructed with about 156,000 asymmetric units selected from 5,873 direct electron detection movies (see Experimental Procedures). The refined helical parameter is different from previously reported ADP-BeFx (Merino et al., 2018) actin structures: the turn per subunit is 167.0 ° (vs. 166.4° for ADP actin and F-actin-Tm complex) (von der Ecken et al., 2015) and the rise per subunit is 27.57 Å. All αhelices and β strands are well defined. Bound ligands and a large portion of the amino acid side chains are resolved in our density map (Figure 4C), permitting atomic modeling of both protein and its ligands. We built and refined to 3.3 Å an atomic model based on this cryoEM map of F-actin and its bound ligands (Figure 4, Supplementary Figure 3). The D-loop in this

structure is elongated, compared to others, making extra connections with neighboring subunits (Figure 5E, Supplementary movie 1).

Phalloidin stabilizes actin by bridging proto-filaments and restricting their relative movement

Phalloidin is a bicyclic heptapeptide, Ala-Trp-Leu (OH) $_2$-Ala-Thr-Cys-Pro (OH), with the sulfur atom of Cys covalently bound to the indole rings of Trp. Its density is well resolved in our map (Figure 5A). Phalloidin binds to F-actin in the cavity between three adjacent protomers, on the side opposite to the H-loop (Figure 5B, Supplementary movie 2). It mainly interacts with two consecutive protomers. The heptapeptide is divided into four sections: one section [Leu(OH)$_2$-Ala-Thr] facing actin i, another (Ala-Trp) facing actin i+1, its hydroxyproline facing the methylated His73, and its cysteine facing empty space between the protomers (Figure 5B, C, D). Interactions between F-actin and phalloidin involve the first two sections of phalloidin. The first section of phalloidin interacts with loop 197–203 of actin i (phalloidin binding loop, named "Φ-loop") mainly through hydrophilic interactions (Figure 5C and 5D). The main chain of its alanine forms multiple hydrogen bonds (dotted lines in Figure 5C and 5D) with the main chain of Gly197-Ser199 of the Φ-loop reminiscent of an antiparallel β-sheet. Hydrogen bonds between phalloidin and Gly197 and Glu 246 reinforce this interaction. The second section, with the sulfur atom of the Cys of phalloidin, inserts into a hydrophobic pocket formed between actin i and i+1. The interaction is mainly hydrophobic, except that Asp179 may form a hydrogen bond with the indole nitrogen of Trp.

Discussion

The goal of this work has been to clarify the role of actin's D-loop dynamics and shape in filament assembly and stability. To this end we used a double cysteine mutant of D-loop, Q41C/V45C (with C374 mutated to S374), in cross-linkings of different span and assessed by light scattering and EM methods its ability to form filaments. The disabled assembly of actin with a short span C41-C45 cross-linking could be rescued by phalloidin. This prompted us to obtain a high-resolution cryoEM structure of F-actin stabilized by phalloidin and BeFx and shed light on how phalloidin compensates for or overcomes local polymerization defects. The inclusion of both phalloidin and BeFx in F-actin was prompted by prior observations of their combined and additive stabilization of filaments as revealed in measurements of their persistence length (Isambert et al., 1995) and melting temperature (Levitsky et al., 2008). Because of the resolution of our cryoEM maps the electron density of BeFx is not identified in the presented images of actin filaments.

D-loop is dynamic and has several structural states

To assess C41-C45 inter-residue distance changes that occur in different nucleotide-bound states of G- and F-actin (in our double mutant Q41C/V45C), we examined several high-resolution actin structures. A helical D-loop state has been reported in the crystal structure of uncomplexed ADP bound G-actin (Otterbein et al., 2001). The Cα-Cα distance between residues 41–45 was 6.2 Å, but it increased to >11 Å in several F-actin structures (Supplementary Figure 2D). It was speculated that this helix to loop change could be

inherent to the transition between ATP and ADP nucleotide states of actin (Otterbein et al., 2001). The helical state of D-loop was not detected in other G-actin crystal structures and thus the loop helix was ascribed to artifacts of crystal contacts (Rould et al., 2006). Yet, molecular dynamics simulations did show the formation of a D-loop helix (Pfaendtner et al., 2009), suggesting that its transient existence may be difficult to capture within current detection methods. To test whether locking the double cysteine mutant across a range of distances may play any significant role in actin dynamics, we utilized a distance based cross-linking approach. Previously, MTS (bifunctional methanothiosulfonate) reagents were used as a molecular ruler to map distances between two cysteine residues placed in several domains of actin and in its D-loop (Oztug Durer et al., 2010). In our case, both disulfide and MTS1/3 cross-linked C41/C45 D-loop mutant was unable to nucleate actin filaments. Supplementing our reactions with F-actin seeds also failed to initiate their elongation. Furthermore, when polymerized mutant actin was treated with Cu^{2+} or MTS1/3 there was rapid filaments destruction. Our results show that the filaments are disrupted or not formed when transient short separations of C41 and C45 (<~6Å) are captured and locked by cross-linking. They imply also that if a helical state of D-loop exists it must be transient. We did not observe any filament disrupting effects when treating actin with MTS6 (~10 Å) or MTS8 (~13 Å) cross-linkers, indicating this to be a favorable separation of C41 and C45 that allows filament formation and stability.

Our results are also consistent with several reported states of D-loop in high-resolution F-actin structures. They suggest changes that can be attributed to a dynamic nature of the filament, and support an open and extended D-loop compared to that in G-actin. Previous biochemical and structural studies support that conclusion. Notable is a striking contrast between filaments disruptive effect of short range cross-linking of a.a. 41–45 (shown in the present work) vs only a minor perturbation of actin polymerization and interactions with myosin following a zero length cross-linking of Q41 to K50 on actin by transglutaminase (Eli-Berchoer L et al., 2000). This latter cross-linking does not constrain the open nature of the D-loop. Consistent with that, the EPR studies and acrylodan labeling experiments suggested that D-loop residues 41, 42, 49, and 50 participate less extensively in filament contacts (Durer et al., 2012). Moreover, EPR experiments with yeast actin and its D-loop residues labeled with spin probes showed their multiple states and mobility, and revealed partial immobilization in F-actin of the probes attached mainly to a.a. 43–47 (Durer et al., 2012). Combined together the present and past results attest to F-actin preference for the open state of the D-loop.

Phalloidin stabilizes actin filaments by inter-subunit contacts

In recent years direct electron counting revolutionized cryoEM analysis of biological samples. This lead to several high-resolution maps (3.2 – 4.6 Å) of F-actin structure (Merino et al., 2018, Chou and Pollard, 2019, Gurel et al., 2017), but some important questions about them remain open. Here, we use high-resolution cryoEM and ADP·BeFx-F-actin-phalloidin to map phalloidin's binding site on actin filaments and reveal how it restricts the relative movement between their two strands and stabilizes F-actin structure. We document important intermolecular contacts in F-actin that are consistent with other high-resolution structures. Although the interaction among protomers along a single filament strand is

relatively strong in the ADP-Pi state (Chou and Pollard, 2019), the two protomers attach to each other with merely two salt bridges: Glu270 of H-loop with Arg39 of D-loop and Glu195 near Φ-loop and Lys113. This configuration is conducive to a variable twist: rectangular structures are prone to shearing or twisting forces. Phalloidin restricts this variability by adding struts that form triangles, which are not easily deformed by such forces. Phalloidin binds actin with a high binding constant ($1.5 + 0.11$)x 10^8 M^{-1}) (De La Cruz and Pollard, 1996). It is likely that its bicyclic structure largely limits its degrees of freedom, and thus compensates for torsional free energy.

On average, each phalloidin molecule has 760 $Å^2$ of surface area buried within actin, almost doubling the inter-protofilament contact (919 $Å^2$ per protomer). This explains how it rescues the assembly of many actin mutants that are defective in their polymerization, as seen here (Figure 2A) and in previous studies (Oztug Durer et al., 2010). We hypothesize that by creating such contacts phalloidin acts as a "super-glue" connecting three actin protomers, thereby stabilizing the filament and bypassing the D-loop anomaly. Our actin-phalloidin structure also reveals additional conformational changes in the D-loop, compared to ADP-BeFx-Factin structure (Merino et al., 2018) (Figure 5E), causing it to extend and establish contacts with residues Tyr148, Thr143, Tyr169, and the C-terminal Phe375 of the neighboring actin. Our structure is consistent with a previous high-resolution actomyosin structure stabilized by phalloidin. The location of phalloidin and the contacts formed by most of the interacting residues are comparable. However, in actomyosin complex phalloidin forms additional contacts compared to those seen in our structure. Those additional interactions may be due to F-actin stabilization by myosin (Mentes et al., 2018). Our structure is also consistent with the manuscript on phalloidin-actin complex structure (Pospich et al., 2020) which became available as this manuscript has undergone revision.

Taken together, our results provide a model (Figure 6) of preferred D-loop state in F-actin based on inter-residue distance-dependent changes in actin polymerization and filaments stability. We show how locking the D-loop residues below an optimal distance between them blocks the transition between G- and F-actin. The fact that intra-loop short-span cross-linkings can occur between a.a.41–45 in F-actin, which result in rapid filament destruction, attests to the dynamic nature of D-loop in the filaments. In addition to that, the high-resolution structure of actin-phalloidin reveals additional contacts made by phalloidin that stabilize actin filaments and help to incorporate polymerization defective monomer units in the filaments.

STAR Methods

RESOURCE AVAILABILITY

Lead Contact—Further information and requests for resources and reagents should be directed to and will be fulfilled by the Lead Contact, Emil Reisler (reisler@mbi.ucla.edu).

Materials Availability—This study did not generate new unique reagents.

Data and Code Availability—3D cryoEM density map has been deposited in the Electron Microscopy Data Bank under the accession number EMD-20694. The coordinates

of atomic model have been deposited in the Protein Data Bank under the accession number 6U96. This study did not generate any new code.

EXPERIMENTAL MODEL AND SUBJECT DETAILS

Saccharomyces cerevisiae C4145 actin mutant strain in pRS314 was used for protein expression and purification (Oztug Durer et al., 2010).

METHOD DETAILS

Purification of yeast actin mutants—Yeast actin was purified essentially as described earlier (Oztug Durer et al., 2010). The protein was eluted from a DNase I affinity column with buffer A (10 mM Tris (pH 7.8), 1 mM DTT, 0.2 mM ATP, and 0.2 mM $CaCl_2$) containing 20–25% sucrose and 50% formamide, and was then applied directly to a DEAE column. Actin was eluted from the DEAE column in the same buffer containing 350 mM KCl. Purified G-actin was dialyzed and stored in buffer B (10 mM HEPES (pH ~7.4), 0.2 mM $CaCl_2$, 0.2 mM ATP, 1.0 mM DTT) on ice.

MTS cross-linking and light scattering—Prior to cross-linking the protein was dialyzed in buffer B supplemented with 0.25mM DTT for ~2 hours followed by 0.1mM DTT for an hour. Immediately after dialysis DTT was removed completely by passing actin through Sephadex G-50 spin columns equilibrated with buffer B (no DTT). The recovered G-actin was then used in the experiments. Actin polymerization, and its disruption due to disulfide cross-linking was monitored via light scattering measurements with the PTI fluorometer (with the excitation and emission wavelengths set at 325nm). Actin polymerization was induced by adding 2.0 mM $MgCl_2$ to G-actin (6.0 μM). Equimolar ratios of phalloidin and MTS reagents to actin, and 2:1 ratio of $CuSO_4$ to actin were added as indicated in figure legends.

Negative stain electron microscopy—Samples collected at various time points were applied to 400-mesh carbon-coated copper grids coated with formvar films (EM Sciences). After 60 seconds of adsorption, the grids were blotted dry and treated with 1% uranyl acetate for 45 seconds. The grids were examined in a Technai T12 electron microscope operated at 120 kV. The collected images were analyzed by using IMAGE J (Schindelin et al., 2012) software.

CryoEM—For cryo electron microscopy (cryoEM) samples of actin were polymerized for 1 h on ice in a buffer containing: 10mM Tris, pH7.4, 0.2mM $CaCl_2$, 50mM KCl, 1.05mM $MgCl_2$, 1mM ATP, 1mM DTT, 0.2mM EGTA. This buffer was supplemented with BeFx (0.2mM $BeCl_2$, 5mM NaF) and equimolar ratio of phalloidin to actin to stabilize the filaments.

Aliquots of 2.5 μL of several F-actin samples were applied onto a "baked" 33 Quantifoil 1.2/1.3 μm, 200 mesh grid, blotted for 4.5 seconds at force 1, then flash-frozen in liquid nitrogen-cooled liquid ethane in a Vitrobot Mark IV (FEI). Grids with frozen-hydrated F-actin were loaded into an FEI Titan Krios electron microscope operated at 300 kV for semi-automated image acquisition with Leginon. CryoEM micrographs were recorded on a Gatan

K2 Summit direct electron detector camera using the electron counting mode at 130,000x nominal magnification (calibrated pixel size of 1.07 Å on the sample level) and defocus values ranging from 2.2 – 4.2 μm. The dose rate on the camera was set to ~8 e/A^2/s. The total exposure time was 8 s, which is fractionated into 32 frames, with 0.25 s exposure time for each frame. We recorded movies (Campbell et al., 2012) of this actin sample with the K2 direct electron detector. Because of the small diameter of F-actin, and the use of 300 keV electrons in cryoEM imaging, individual frames of direct electron counting movies do not have sufficient signal to be aligned directly. Therefore, we added 10 nm gold particles to the sample, which are prominently visible in Figure 4A, in order to generate a fiducial signal for frame alignment. The gold particles and Fresnel fringes around them enabled us to align the individual frames in most of the movies and to determine their defocus parameters.

Image processing and atomic modeling—The movies were aligned and averaged for correction of beam-induced drift using the GPU-accelerated program MotionCorr (Li et al., 2013). The average images from all frames were used for defocus determination and particle picking, and those from the first 16 frames (corresponding to ~30 e$^-$/Å2 total dose on sample) were aligned and summed to produce a micrograph for 2D and 3D image classification. From the total of 5,874 movies recorded in a continuous session, we selected the best 2,865 micrographs for in-depth data processing.

We manually picked 6,761 actin segments from selected micrographs by EMAN (Tang et al., 2007) helixboxer, and segmented them into 214,583 boxes of 360×360 pixels by 10% interbox distance. We used Relion Class2D and Class3D to eliminate bad particles. The Iterative Helical Real-Space Refinement (IHRSR) method (Egelman, 2010) as implemented within the Relion 3 (He and Scheres, 2017) framework was used to process the selected particles for high-resolution reconstruction. The final, helical cryoEM density map was calculated from 181,627 selected particles with Refine3D, to a resolution of 3.8 Å. We then re-extracted sub-particles (96×96 boxes) from these selected particles and finely adjusted their orientation and center parameters locally. The resolution of the newly reconstructed, sub-particle map was determined to be 3.3 Å based on the "gold-standard" FSC criterion. Atomic model of actin was initially built with Coot (Emsley and Cowtan, 2004) and refined with Phenix real_space_refine (Adams et al., 2010).

QUANTIFICATION AND STATISTICAL ANALYSIS

Graphs were plotted using Sigmaplot v14 (from Systat Software, Inc., San Jose California USA, www.systatsoftware.com). Figures containing CryoEM map and model were generated using Chimera (Pettersen et al., 2004). All biochemical experiments were repeated for at least 3 times (n=3).

Supplementary Material

Refer to Web version on PubMed Central for supplementary material.

Acknowledgements

Reference

Adams PD, Afonine PV, Bunkóczi G, Chen VB, Davis IW, Echols N, Headd JJ, Hung L-W, Kapral GJ, Grosse-Kunstleve RW, et al. (2010). PHENIX : a comprehensive Python-based system for macromolecular structure solution. Acta Crystallogr. D Biol. Crystallogr. 66, 213–221. [PubMed: 20124702]

Campbell MG, Cheng A, Brilot AF, Moeller A, Lyumkis D, Veesler D, Pan J, Harrison SC, Potter CS, Carragher B, et al. (2012). Movies of ice-embedded particles enhance resolution in electron cryo-microscopy. Struct. Lond. Engl. 1993 20, 1823–1828.

Chou SZ, and Pollard TD (2019). Mechanism of actin polymerization revealed by cryo-EM structures of actin filaments with three different bound nucleotides. Proc. Natl. Acad. Sci. 116, 4265–4274. [PubMed: 30760599]

Dalhaimer P, Pollard TD, and Nolen BJ (2008). Nucleotide-mediated conformational changes of monomeric actin and Arp3 studied by molecular dynamics simulations. J. Mol. Biol. 376, 166–183. [PubMed: 18155236]

De La Cruz EM, and Pollard TD (1996). Kinetics and thermodynamics of phalloidin binding to actin filaments from three divergent species. Biochemistry 35, 14054–14061. [PubMed: 8916890]

Durer ZAO, Kudryashov DS, Sawaya MR, Altenbach C, Hubbell W, and Reisler E (2012). Structural states and dynamics of the D-loop in actin. Biophys. J. 103, 930–939. [PubMed: 23009842]

von der Ecken J, Müller M, Lehman W, Manstein DJ, Penczek PA, and Raunser S (2015). Structure of the F-actin–tropomyosin complex. Nature 519, 114–117. [PubMed: 25470062]

Egelman EH (2010). Reconstruction of Helical Filaments and Tubes. In Methods in Enzymology, 495 (Elsevier), pp. 167–183.

Eli-Berchoer L, Reisler, and Muhlrad (2000). Effect of intramolecular cross-linking between glutamine-41 and lysine-50 on actin structure and function. J Muscle Res Cell Motil 78(3, 405–414.

Emsley P, and Cowtan K (2004). Coot : model-building tools for molecular graphics. Acta Crystallogr. D Biol. Crystallogr. 60, 2126–2132. [PubMed: 15572765]

Galkin VE, Orlova A, Vos MR, Schröder GF, and Egelman EH (2015). Near-Atomic Resolution for One State of F-Actin. Structure 23, 173–182. [PubMed: 25533486]

Ge P, Durer ZAO, Kudryashov D, Zhou ZH, and Reisler E (2014). Cryo-EM reveals different coronin binding modes for ADP– and ADP–BeFx actin filaments. Nat. Struct. Mol. Biol. 21, 1075–1081. [PubMed: 25362487]

Graceffa P, and Dominguez R (2003). Crystal structure of monomeric actin in the ATP state. Structural basis of nucleotide-dependent actin dynamics. J. Biol. Chem. 278, 34172–34180. [PubMed: 12813032]

Grintsevich EE, Ge P, Sawaya MR, Yesilyurt HG, Terman JR, Zhou ZH, and Reisler E (2017). Catastrophic disassembly of actin filaments via Mical-mediated oxidation. Nat. Commun. 8, 2183. [PubMed: 29259197]

Gurel PS, Kim LY, Ruijgrok PV, Omabegho T, Bryant Z, and Alushin GM (2017). Cryo EM structures reveal specialization at the myosin VI-actin interface and a mechanism of force sensitivity. ELife 6.

He S, and Scheres SHW (2017). Helical reconstruction in RELION. J. Struct. Biol. 198, 163–176. [PubMed: 28193500]

Isambert H, Venier P, Maggs AC, Fattoum A, Kassab R, Pantaloni D, and Carlier MF (1995). Flexibility of actin filaments derived from thermal fluctuations. Effect of bound nucleotide, phalloidin, and muscle regulatory proteins. J. Biol. Chem. 270, 11437–11444. [PubMed: 7744781]

Kabsch W, Mannherz HG, Suck D, Pai EF, and Holmes KC (1990). Atomic structure of the actin:DNase I complex. Nature 347, 37–44. [PubMed: 2395459]

Kim E, and Reisler E (1996). Intermolecular coupling between loop 38–52 and the C-terminus in actin filaments. Biophys. J. 71, 1914–1919. [PubMed: 8889166]

Kim E, Phillips M, Hegyi G, Muhlrad A, and Reisler E (1998). Intrastrand Cross-Linked Actin between Gln-41 and Cys-374. II. Properties of Cross-Linked Oligomers †. Biochemistry 37, 17793–17800. [PubMed: 9922145]

Kotila T, Kogan K, Enkavi G, Guo S, Vattulainen I, Goode BL, and Lappalainen P (2018). Structural basis of actin monomer re-charging by cyclase-associated protein. Nat. Commun. 9.

Laskowski RA, and Swindells MB (2011). LigPlot+: Multiple Ligand–Protein Interaction Diagrams for Drug Discovery. J. Chem. Inf. Model. 51, 2778–2786. [PubMed: 21919503]

Levitsky DI, Pivovarova AV, Mikhailova VV, and Nikolaeva OP (2008). Thermal unfolding and aggregation of actin: Stabilization and destabilization of actin filaments. FEBS J. 275, 4280–4295. [PubMed: 18637820]

Li X, Mooney P, Zheng S, Booth CR, Braunfeld MB, Gubbens S, Agard DA, and Cheng Y (2013). Electron counting and beam-induced motion correction enable near-atomic-resolution single-particle cryo-EM. Nat. Methods 10, 584–590. [PubMed: 23644547]

McLaughlin PJ, Gooch JT, Mannherz HG, and Weeds AG (1993). Structure of gelsolin segment 1-actin complex and the mechanism of filament severing. Nature 364, 685–692. [PubMed: 8395021]

Mentes A, Huehn A, Liu X, Zwolak A, Dominguez R, Shuman H, Ostap EM, and Sindelar CV (2018). High-resolution cryo-EM structures of actin-bound myosin states reveal the mechanism of myosin force sensing. Proc. Natl. Acad. Sci. U. S. A. 115, 1292–1297. [PubMed: 29358376]

Merino F, Pospich S, Funk J, Wagner T, Küllmer F, Arndt H-D, Bieling P, and Raunser S (2018). Structural transitions of F-actin upon ATP hydrolysis at near-atomic resolution revealed by cryo-EM. Nat. Struct. Mol. Biol. 25, 528–537. [PubMed: 29867215]

Neuhaus JM, Wanger M, Keiser T, and Wegner A (1983). Treadmilling of actin. J. Muscle Res. Cell Motil. 4, 507–527. [PubMed: 6358256]

Oda T, Namba K, and Maéda Y (2005). Position and Orientation of Phalloidin in F-Actin Determined by X-Ray Fiber Diffraction Analysis. Biophys. J. 88, 2727–2736. [PubMed: 15653738]

Oda T, Iwasa M, Aihara T, Maéda Y, and Narita A (2009). The nature of the globular- to fibrous-actin transition. Nature 457, 441–445. [PubMed: 19158791]

Orlova A, and Egelman EH (1992). Structural basis for the destabilization of F-actin by phosphate release following ATP hydrolysis. J. Mol. Biol. 227, 1043–1053. [PubMed: 1433285]

Otterbein LR, Graceffa P, and Dominguez R (2001). The crystal structure of uncomplexed actin in the ADP state. Science 293, 708–711. [PubMed: 11474115]

Otterbein LR, Cosio C, Graceffa P, and Dominguez R (2002). Crystal structures of the vitamin D-binding protein and its complex with actin: structural basis of the actin-scavenger system. Proc. Natl. Acad. Sci. U. S. A. 99, 8003–8008. [PubMed: 12048248]

Oztug Durer ZA, Diraviyam K, Sept D, Kudryashov DS, and Reisler E (2010). F-actin structure destabilization and DNase I binding loop: fluctuations mutational cross-linking and electron microscopy analysis of loop states and effects on F-actin. J. Mol. Biol. 395, 544–557. [PubMed: 19900461]

Paavilainen VO, Bertling E, Falck S, and Lappalainen P (2004). Regulation of cytoskeletal dynamics by actin-monomer-binding proteins. Trends Cell Biol. 14, 386–394. [PubMed: 15246432]

Pettersen EF, Goddard TD, Huang CC, Couch GS, Greenblatt DM, Meng EC, and Ferrin TE (2004). UCSF Chimera?A visualization system for exploratory research and analysis. J. Comput. Chem. 25, 1605–1612. [PubMed: 15264254]

Pfaendtner J, Branduardi D, Parrinello M, Pollard TD, and Voth GA (2009). Nucleotide dependent conformational states of actin. Proc. Natl. Acad. Sci. 106, 12723–12728. [PubMed: 19620726]

Pollard TD (2016). Actin and Actin-Binding Proteins. Cold Spring Harb. Perspect. Biol. 8.

Pollard TD (2017). What We Know and Do Not Know About Actin. Handb. Exp. Pharmacol. 235, 331–347. [PubMed: 27873086]

Pospich S, Merino F, and Raunser S (2020). Structural Effects and Functional Implications of Phalloidin and Jasplakinolide Binding to Actin Filaments. Structure.

Robinson RC, Mejillano M, Le VP, Burtnick LD, Yin HL, and Choe S (1999). Domain movement in gelsolin: a calcium-activated switch. Science 286, 1939–1942. [PubMed: 10583954]

Rould MA, Wan Q, Joel PB, Lowey S, and Trybus KM (2006). Crystal structures of expressed non-polymerizable monomeric actin in the ADP and ATP states. J. Biol. Chem. 281, 31909–31919. [PubMed: 16920713]

Saunders MG, Tempkin J, Weare J, Dinner AR, Roux B, and Voth GA (2014). Nucleotide regulation of the structure and dynamics of G-actin. Biophys. J. 106, 1710–1720. [PubMed: 24739170]

Schindelin J, Arganda-Carreras I, Frise E, Kaynig V, Longair M, Pietzsch T, Preibisch S, Rueden C, Saalfeld S, Schmid B, et al. (2012). Fiji: an open-source platform for biological image analysis. Nat. Methods 9, 676–682. [PubMed: 22743772]

Shvetsov A, Stamm JD, Phillips M, Warshaviak D, Altenbach C, Rubenstein PA, Hideg K, Hubbell WL, and Reisler E (2006). Conformational Dynamics of Loop 262–274 in G- and F-actin [†]. Biochemistry 45, 6541–6549. [PubMed: 16700564]

Suarez C, Roland J, Boujemaa-Paterski R, Kang H, McCullough BR, Reymann A-C, Guérin C, Martiel J-L, De La Cruz EM, and Blanchoin L (2011). Cofilin Tunes the Nucleotide State of Actin Filaments and Severs at Bare and Decorated Segment Boundaries. Curr. Biol. 21, 862–868. [PubMed: 21530260]

Tang G, Peng L, Baldwin PR, Mann DS, Jiang W, Rees I, and Ludtke SJ (2007). EMAN2: An extensible image processing suite for electron microscopy. J. Struct. Biol. 157, 38–46. [PubMed: 16859925]

Tirion MM, and ben-Avraham D (1993). Normal mode analysis of G-actin. J. Mol. Biol. 230,186–195. [PubMed: 8450535]

Zheng X, Diraviyam K, and Sept D (2007). Nucleotide Effects on the Structure and Dynamics of Actin. Biophys. J. 93, 1277–1283. https://systatsoftware.com/ [PubMed: 17526584]

Highlights

- Structure-function insights into actin as revealed by Cryo-EM and Light Scattering.

- D-loop dynamics and its effect on filament assembly and stability.

- Phalloidin rescues the assembly of defective cross-linked G-actin D-loop mutant.

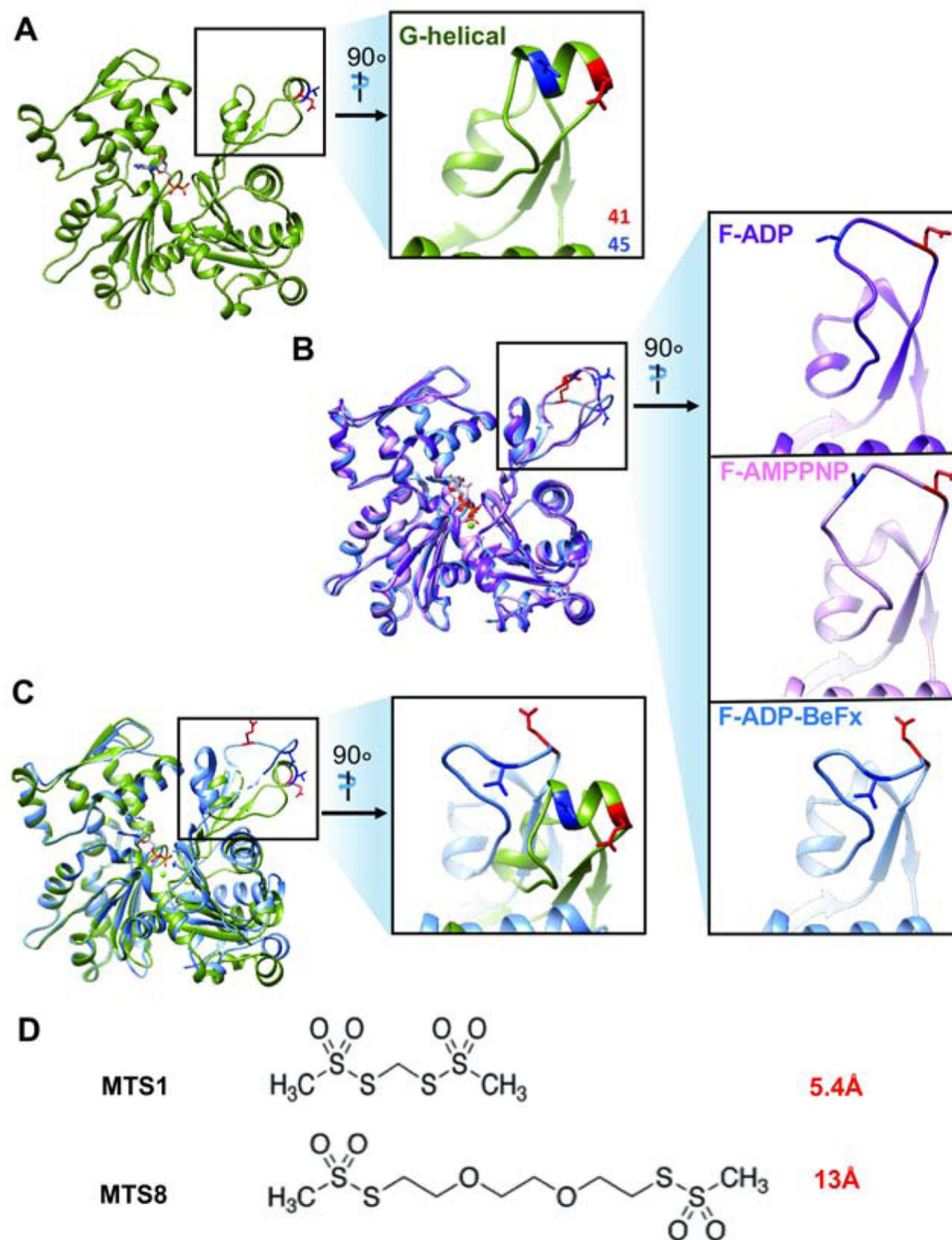- Phalloidin stabilize the actin assembly by allowing inter-protomer D-loop contacts.

Figure 1. D-loop flexibility depends on the nucleotide state of actin.
Comparison of D-loops in different F-actin structures with a helical D-loop (1J6Z.pdb) in G-actin (A). (B) High resolution cryoEM structures of F-actin with the bound ADP (6DJO.pdb), AMPPNP (6DJM.pdb), and ADP+BeFx (5OOF.pdb) show the corresponding loop states. (C) Comparison of G-actin D-loop conformations in the helical state and in ADP-BeFx-F-actin. In both forms, residues 41 and 45 are marked in red and blue, respectively. For 90 degree rotated close-up images some regions of actin structure have

been clipped by Chimera for visual clarity. (D) MTS1 and MTS8 reagents and their crosslinking distances.
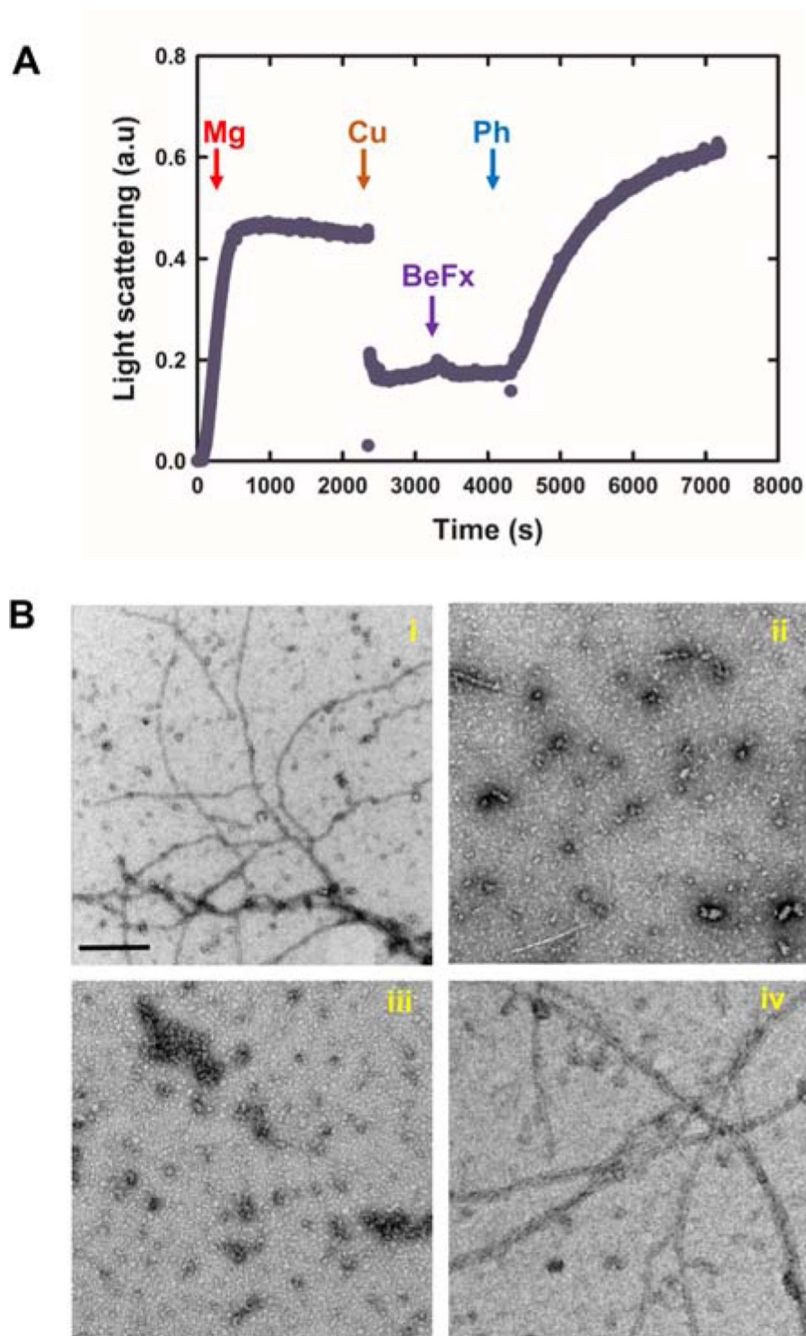
Figure 2. Phalloidin rescues the polymerization of oxidized D-loop actin mutant C41/C45.
(A) The polymerization of yeast actin mutant C41/C45 by 2 mM $MgCl_2$ was monitored by
light scattering measurements. At the polymerization plateau 20 μM $CuSO_4$ was added to F-
actin (orange arrow) to catalyze disulfide bond formation between C41 and C45. This
resulted in filaments disassembly. Subsequent addition of BeFx (purple arrow) did not
restore the filaments, but they were reformed upon addition of equimolar phalloidin (green
arrow). (B) Electron micrographs of C41/C45 actin collected after additions of: (i) Mg, to G-
actin (ii) $CuSO_4$ to C41/C45 F-actin shown in (i), (iii) Mg followed by $CuSO_4$ and then

followed by BeFx, and (iv) Mg, CuSO$_4$, BeFx, and phalloidin (in that order). Electron microscopy samples were taken from experiments run in parallel to those shown in A. For control filaments, 10 mM DTT was added to block disulfide bond formation. The scale bar in image (i) corresponds to 0.2 μm.
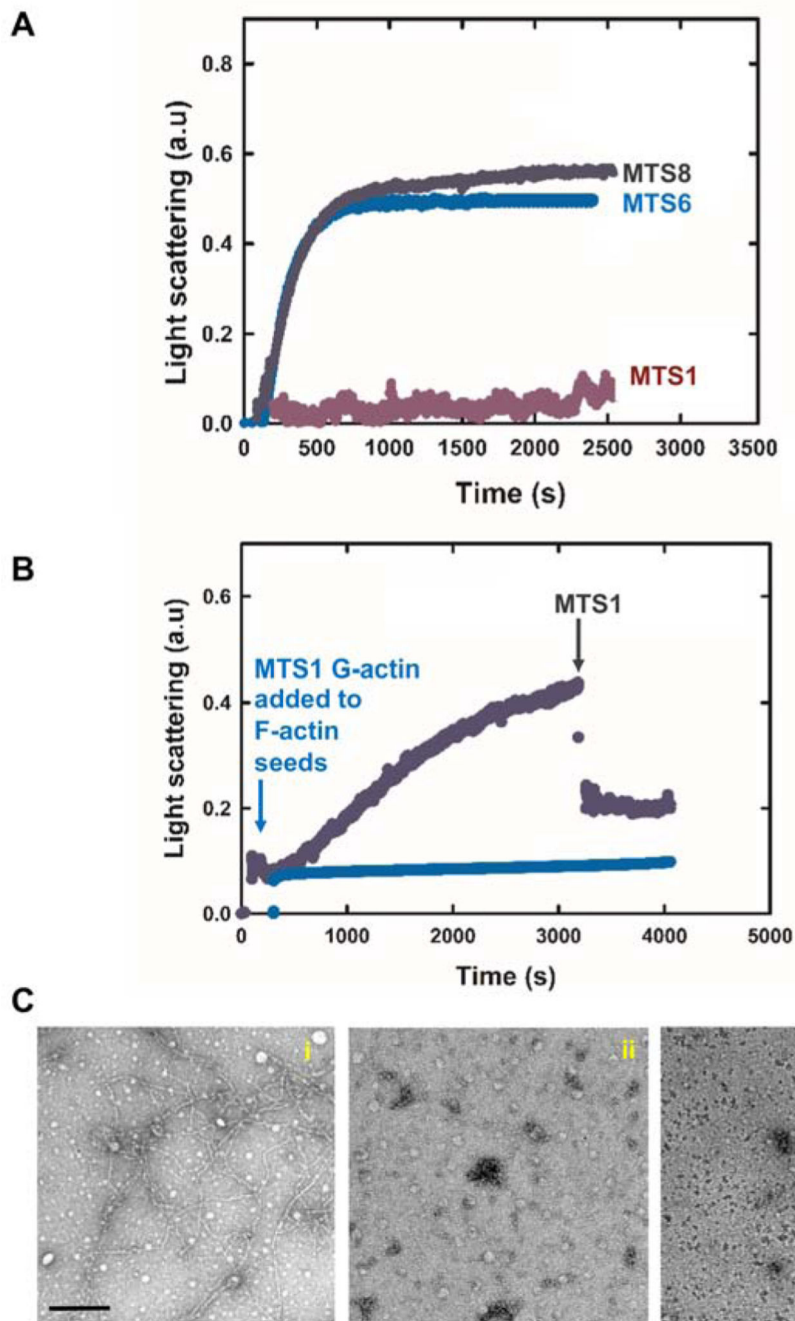
Figure 3. Cross-linking span dependent polymerization/depolymerization of actin D-loop double mutant C41/C45.

(A) Yeast F-actin C41/C45 mutant was cross-linked with equimolar MTS1 (purple)-, MTS6 (blue) or MTS8 (grey), (with their mean respective cross-linking distances of ~5.4 Å, 10 Å, and 13 Å), and its polymerization by 2 mM MgCl$_2$ was monitored by light scattering measurements. (B) Yeast F-actin C41/C45 was depolymerized with the addition of equimolar MTS1. MTS1 cross-linked G-actin failed to polymerize in the presence of control actin filament seeds and 2 mM MgCl$_2$ (as monitored by light scattering). (C) Electron micrographs of actin-C41/C45 after additions of: (i) MTS8 and Mg (filaments are formed);

(ii) MTS1 and Mg – no filaments formation; and (iii) MTS1 addition to F-actin (filaments are not detected). Electron microscopy samples were taken from experiments ran in parallel to those shown in A and B. The scale bar in EM images corresponds to 0.2 μm.
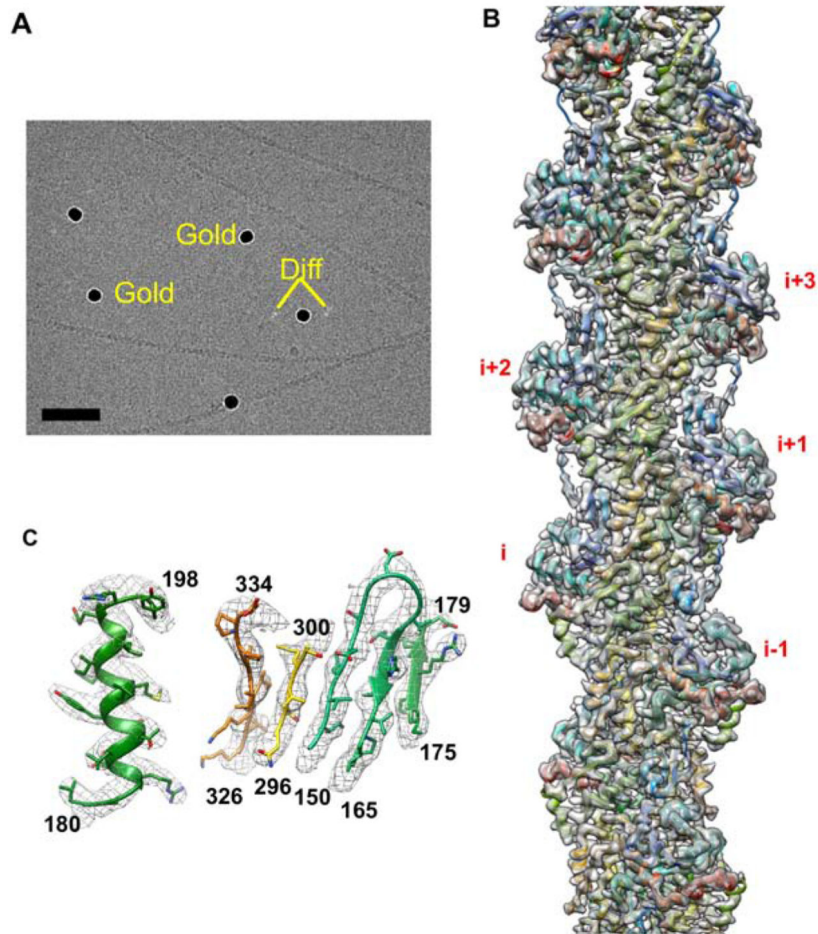
Figure 4: CryoEM structure of ADP-BeF$_x$-F-actin-phalloidin.

(A) An average image of an aligned representative direct electron detector movie (stack). Bar: 400 Å; Gold: 10 nm gold particles; Diff: diffraction contrast generated by the lattice of gold particles. (B) Overall structure of ADP-BeF$_x$-F-actin-phalloidin at 3.3 Å resolution, fitted with atomic model of G-actin. Notations in red indicate the relative position of actin monomers in the filament. (C) Representative regions (marked by amino acid numbers) of the density map fitted with their atomic models, showing the quality of the map. Actin in B and C is shown in Chimera rainbow colors
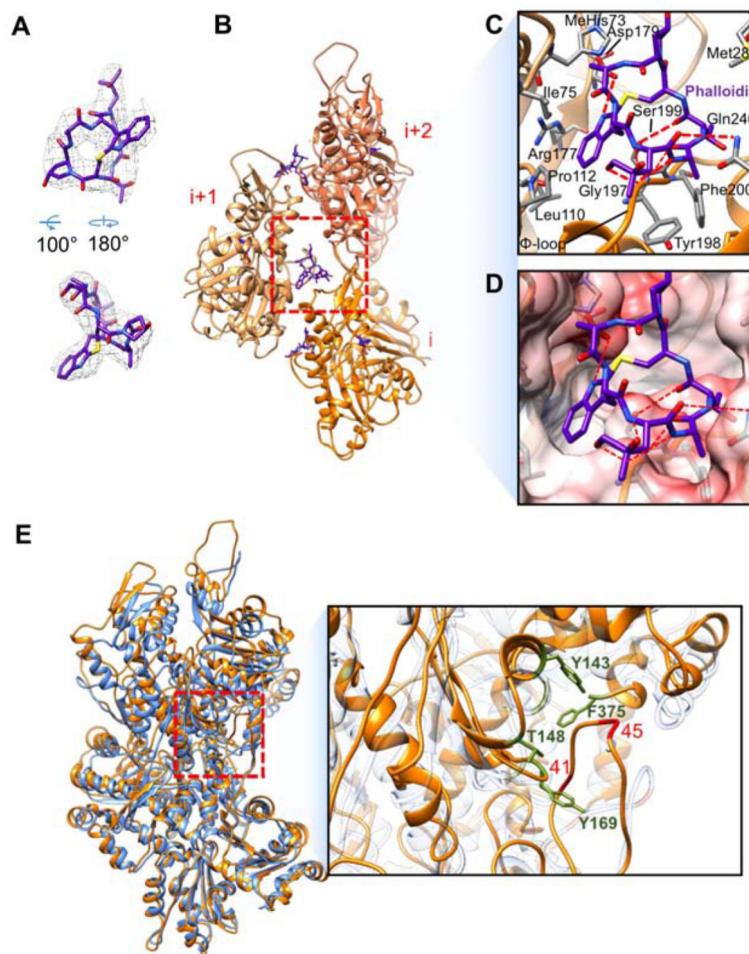
Figure 5: F-actin structure and interactions with phalloidin

(A) Chemical structure and atomic model of phalloidin (sticks) as resolved by our cryo-EM structure (mesh). The four sections of phalloidin are shown by colored blocks. (B) Placement of phalloidin among actin protomers in the filament, with protomer units numbered in red. (C and D) Close-up of interaction between phalloidin (sticks model) and actin (ribbon and stick in B, and molecular surface colored by Coulomb potential using Chimera in D). In all panels, the stick models for atoms are colored: red for O; blue for N; yellow for S; C atoms follow the color of the model. Hydrogen bonds are shown as red dotted lines. (E) Phalloidin enhances inter-protomer D-loop contacts. To compare two D-loop regions ADP-BeFx-F-actin (5OOF.pdb) was superimposed on our ADP-BeFx-F-actin-phalloidin structure with Chimera. In the inset a 3.5 Å zone around D-loop residues 41–45 was chosen with Chimera and residues making contacts in our cryo-EM structure are shown by the stick option of Chimera. The published structure of BeFx-F-Actin was made slightly transparent for visual clarity.
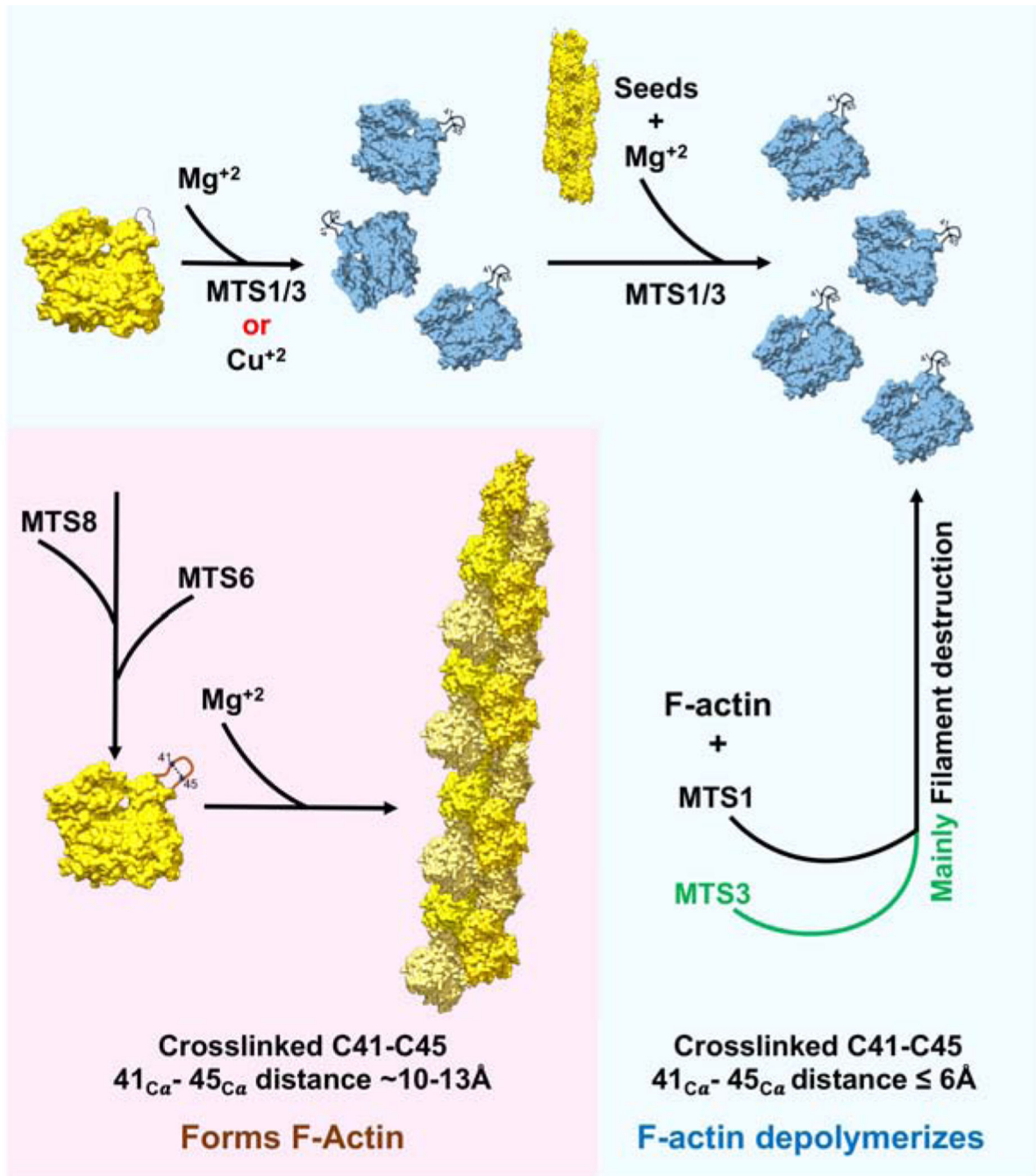
Figure 6: Model representation of the effects of variable distance cross-linkings of C41 and C45 in yeast actin mutant on filaments formation or destruction

KEY RESOURCES TABLE

REAGENT or RESOURCE	SOURCE	IDENTIFIER
Antibodies		
Bacterial and Virus Strains		
Biological Samples		
Chemicals, Peptides, and Recombinant Proteins		
Uranyl Formate	EM Sciences	Cat#22450
1,1-Methanediyl Bismethanethiosulfonate (MTS-1)	Toronto Research Chemicals	M258800
1,3-Propanediyl Bismethanethiosulfonate (MTS-3)	Toronto Research Chemicals	P760350
1,6-Hexanediyl Bismethanethiosulfonate (MTS-6)	Toronto Research Chemicals	H294250
1,8-Octadiyl Bismethanethiosulfonate (MTS-8)	Toronto Research Chemicals	O235850
Deoxyribonuclease I (DNase I)	Worthington Biochemical	LS002139
Affi-Gel 10 Gel	BioRad	1536099
Critical Commercial Assays		
Deposited Data		
Actin phalloidin at BeFx state	This paper	PDB: 6U96
Actin phalloidin at BeFx state	This paper	EMDB: 20694
F-actin in complex with ADP-BeFx	Merino et al.,2018	PDB: 5OOF
Uncomplexed actin in the ADP state	Otterbein et al., 2001	PDB: 1J6Z
Structure of ADP-actin filaments	Chou and Pollard, 2019	PDB: 6DJO
Structure of AMPPNP-actin filaments	Chou and Pollard, 2019	PDB: 6DJM
Experimental Models: Cell Lines		
Experimental Models: Organisms/Strains		
Saccharomyces cerevisiae C4145 mutant strain in pRS314	Dr. Reisler's lab, this paper	C41-C45
Oligonucleotides		
Recombinant DNA		
Software and Algorithms		
CHIMERA	Pettersen et al., 2004	https://www.cgl.ucsf.edu/chimera/download.html
RELION 3.0	He and Scheres, 2017	https://www3.mrc-lmb.cam.ac.uk/relion
Coot	Emsley and Cowtan, 2004	https://www2.mrc-lmb.cam.ac.uk/personal/pemsley/coot/
MotionCorr	Li et al., 2013	https://emcore.ucsf.edu/ucsf-motioncor2
Phenix	Adams et al., 2010	https://www.phenix-online.org/
ImageJ	Schindelin et al., 2012	https://imagej.net/ImageJ

REAGENT or RESOURCE	SOURCE	IDENTIFIER
EMAN	Tang et al.,2007	http://blake.bcm.tmc.edu/EMAN2/
Sigmaplot14	Systat Software, Inc., San Jose California USA	https://systatsoftware.com/products/sigmaplot/
LigPlot+	Laskowski and Swindells, 2011	https://www.ebi.ac.uk/thornton-srv/software/LigPlus/
Other		
Gilder Copper grids, 400 Mesh	Ted Pella	Cat#G400